JOURNAL OF MATERIALS SCIENCE 30 (1995) 2121–2129

Microstructure and mechanical properties of spherical zirconia–yttria granules

W. PYDA, M. S. J. GANI*
*Centre for Bioprocess Technology and *Department of Materials Engineering, Monash University, Clayton 3168, Victoria, Australia*

The methods used to prepare three spray dried yttria–zirconia powders have been shown to have a large effect on their behaviour during subsequent heat treatment and also on their resultant properties. Changes of morphology of the granules, their surface area, pore size distribution, porosity and compressive strength which occur during heat treatment have been determined. A concept of local densification was used to explain the observed changes in pore size distribution, where it was shown that distributions with pores smaller than 60–80 nm resulted in significant pore enlargement during the early stages of sintering. A theory based on fracture mechanics explained the changes in compressive strength of the granules.

1. Introduction

Ceramic powders are widely used for many applications. These include powders used as starting materials for the production of traditional and fine ceramics [1–3], as materials for ultrafiltration [4], catalysts [5] and chromatography [5, 6]. The powder characteristics required are dependent on the application, for example, in the production of fine ceramics it is desirable to produce a sintered ceramic of low porosity and fine grain size, since these two factors influence the mechanical properties of the ceramic. In this case it is desirable that the agglomerates of particles that occur in most powders have low strength ("soft" agglomerates) so that they will deform and breakdown during the compaction process prior to firing, and thus not lead to residual porosity or excessive grain growth in the fired product [7–9]. However, agglomerates that are to be used as catalysts or catalyst support materials, are required to maintain both high surface area and porosity at elevated temperatures. These two characteristics are also required for powders used in liquid chromatography, but in this case there is the additional requirement of high compressive strength, so that they can withstand the high pressures which are involved in the packing of columns [10].

The aim of this investigation is to produce spherical granules that have sufficient strength, surface area and porosity to enable their use in chromatography, and to investigate how the changes in morphology and properties, that occur during sintering, are determined by the method of preparation of the starting materials prior to spray drying. One yttria–zirconia powder was prepared from an original wet amorphous gel, the second from an attrition milled predried gel, and the third from a calcined crystalline material.

2. Experimental procedure

Two zirconia–8 mol % yttria powders were prepared by coprecipitation of a gel from a vigorously stirred mixture of aqueous solutions of zirconium tetrachloride (assay 98%) and yttrium oxide (assay 99.9%) in HCl with ammonia Fig. 1. The final pH was maintained at 9. The gel was washed until free of Cl^- ions, and then divided into two parts, the first of which was used for the preparation of a slurry to spray drying (sample W) and the second was dried at 120 °C and attrition milled in water for 3 h using 0.8 mm diameter zirconia balls (sample G). Both gels (17.0 ± 0.2 wt % in water) were then spray dried using a Niro atomizer, with inlet and outlet temperatures of 280 ± 5 and 100 ± 3 °C, respectively. The third powder (sample C) was a coprecipitated, zirconia–2.85 mol % yttria spray dried precalcined (1000 °C) powder.

Heat treatment of the powders was carried out at temperatures from 500 to 1400 °C in air, at a heating and cooling rate of 50 °C min^{-1}, with a 2 h soak at temperature. The morphology and granule size distributions were determined from scanning electron micrographs obtained for a Jeol JSM-840A scanning electron microscope (SEM). Transmission electron micrographs (Philips EM420) were used for the measurement of agglomerate and aggregate size distributions. A Zeiss particle size analyser was used to measure a population of about 2000 particles in each sample. X-ray diffraction traces (Rigaku) were used to identify the crystalline phases and also the crystallite sizes, which were obtained from the Scherrer formula, with corrections for the α_1 and α_2 overlap, and instrumental line broadening [11]. The specific surface area, from which the equivalent particle size was calculated, was determined by the Brunauer–Emmett–Teller (BET) method using a Micromeritics Gemini 2360.

0022–2461 © *1995 Chapman & Hall*

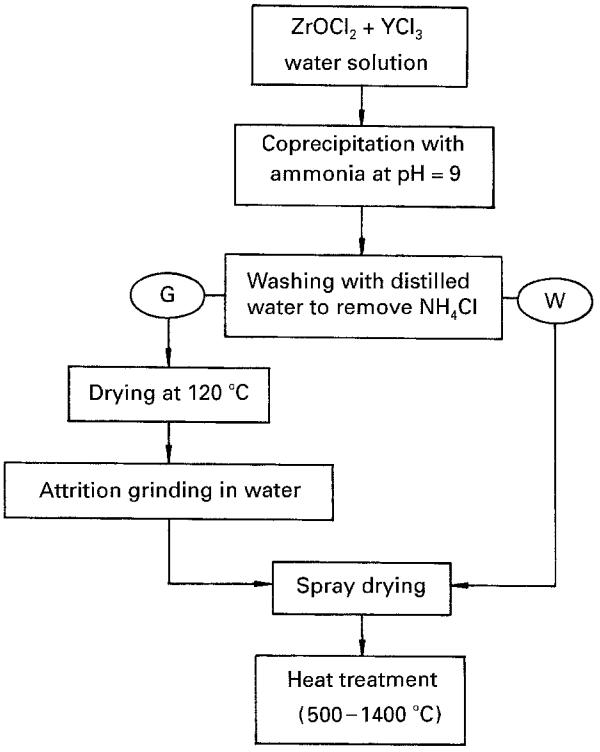

Figure 1 Schematic diagram of the powder preparation route.

A mercury porosimeter (Micromeritic Poresizer 9310) was used for pore size measurements for pores of diameter $\geqslant 7.5$ nm. The total porosity of the granules was calculated on the basis of their volume derived from these measurements and the volume occupied by the solid phase. The amount of pores smaller than 7.5 nm and/or closed pores were found from the difference between these two measurements. The compressive strength of the granules was determined by measurement of the densification of the powders as a function of increasing uniaxial pressure [7, 12, 13]. An Instron 4505 testing machine was used to compress the powders contained in a 10 mm diameter steel mould. The loading rate was 1 mm min^{-1} to a maximum load of 31.5 kN. The calculated compact density was corrected for elastic deformation of the mould and the powder. The compressive strength was found from breakpoints in a log–log plot of density versus log of the compaction pressure. X-ray diffraction (XRD) measurements of the lattice parameters were used to calculate the densities of the Y_2O_3–ZrO_2 solid solutions [14], and the density of the gels were found to be 3.71 ± 0.04 g cm^{-3}, using a pycnometer in ethyl alcohol.

3. Results and discussion

3.1. Powders before heat treatment

There were significant differences between the physical characteristics of the powders that were used to form the granules, and also in the spray dried granules, as shown in Table I, and the morphology and size distributions as illustrated in Figs 2 and 3. Sample G (the dried attrition milled gel) was composed of porous, high surface area amorphous gel agglomerates made up of 5–7 nm particles [15], whereas C (the precalcined powder) consisted of aggregates of fine, dense crystalline particles. C had a narrower particle size distribution, smaller particle size (Fig. 3) and a smaller specific surface area (Table I) than the powder G. The large granule size of the powder C after spray drying could be due to the use of a more concentrated slurry, in that a value of 14 vol % could easily be achieved in this case; whereas the slurries prepared from the gels exhibited a viscosity suitable for spray drying when they contained only 5–10 vol % of particles. Granules of G and C had similar morphology, in that they exhibited a distinct substructure in the agglomerates (Fig. 4), whereas granules prepared W (the wet gel) were characterized by smooth surfaces with some evidence of cracking. The latter granules had the highest specific surface area and smallest total porosity.

TABLE I Properties of the attrition milled and spray dried powders

Property	Sample G	Sample W	Sample C
Attrition milled powders			
Range of agglomerate size, μm	0.02–0.74		0.01–0.25
Agglomerate size, d_{50}, μm	0.40		0.14
mode, μm	0.09		0.07
Specific surface area, $m^2 g^{-1}$	99.5 ± 3.6[a]		14.4 ± 0.5
d_{BET}, nm	16.3 ± 0.6		68.4 ± 2.3
Spray dried powders			
Range of granule size, μm	1.8–27.7	1.2–26.6	3.7–77.8
Granule size, d_{50}, μm	17.8	14.8	43.4
mode, μm	6.4	5.6	16.0
Specific surface area, $m^2 g^{-1}$	93.5 ± 2.9	143.0 ± 5.7	14.4 ± 0.5
d_{BET}, nm	17.3 ± 0.5	11.3 ± 0.4	68.4 ± 2.3
Compressive strength, MPa			
Granules	0.15 ± 0.05	14.0 ± 0.8	0.26 ± 0.06
Agglomerates	125 ± 12	132 ± 10	–
Total porosity, vol. %	66.0 ± 1.4	33.0 ± 0.8	63.9 ± 1.2
Amount of pores > 7.5 nm	57.6 ± 1.3	7.0 ± 1.0	54.7 ± 1.4
Phase composition, vol. %	Amorphous	Amorphous	51.1 m + 48.9 t[b]

[a] $\pm$ denotes the confidence interval at a confidence level of 0.95 in the entire work.
[b] m and t denote zirconia solid solution of monoclinic and tetragonal symmetry, respectively.

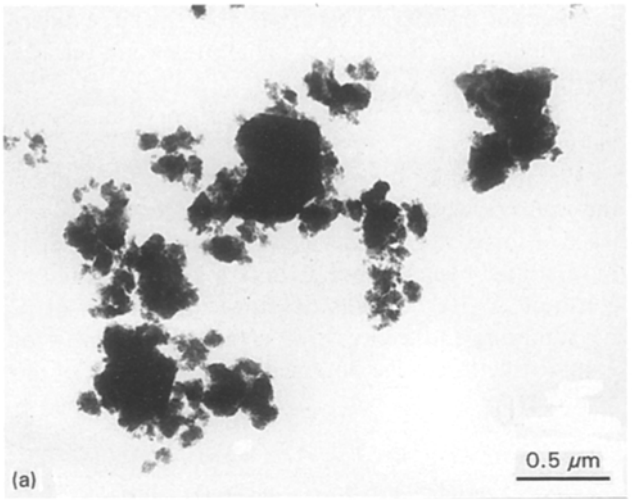

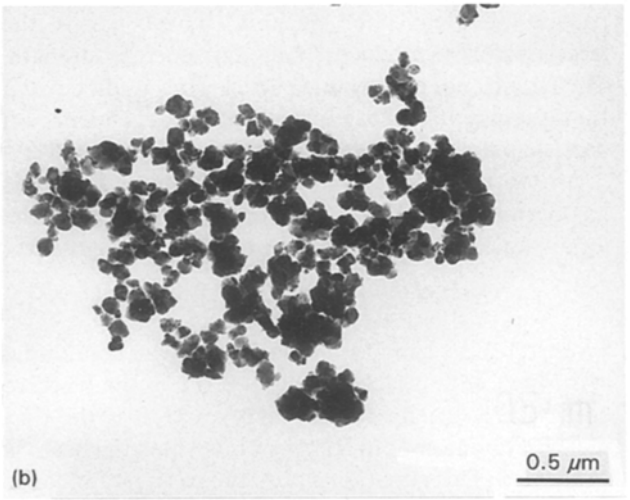

Figure 2 TEM micrographs of the attrition milled powders: (a) amorphous gel of sample G, (b) crystalline aggregates of sample C.

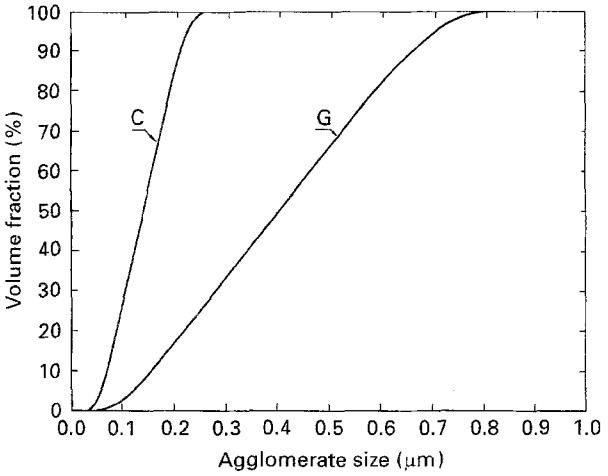

Figure 3 Cumulative particle size distribution curves for the attrition milled powders.

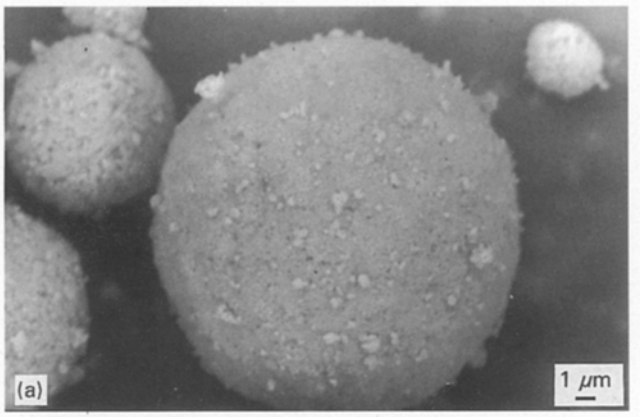

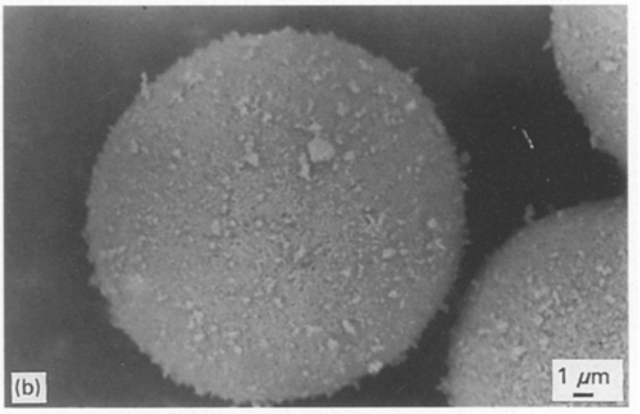

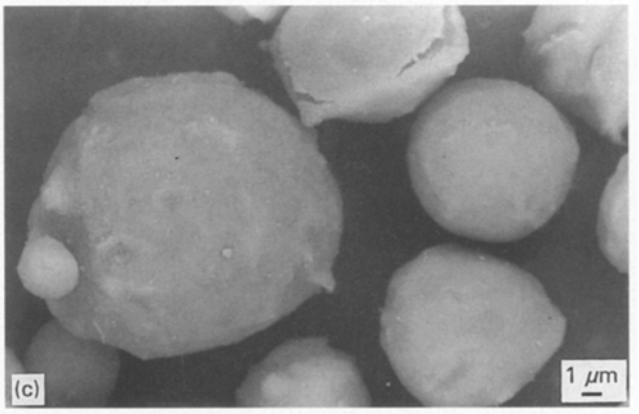

Figure 4 Backscattered SEM micrographs of the granules after spray drying: (a) sample G, (b) sample C, and (c) sample W.

The pore size distributions of the powders are shown in Fig. 5. Distinct pore populations were observed within the granules of G and C, which are formed from interagglomerate pores (G) and/or interaggregate pores (C). The larger agglomerate sizes and the broader agglomerate size distribution of the attrition milled gel (G), Fig. 3, resulted in larger pore sizes and a broader pore size distribution in the spray dried powder. The intraagglomerate pores in G were too small to be penetrated by mercury, as was indicated by results reported in [16]. This is also suggested by a small difference between the amount of pores intruded during the porosimetry measurement ($d > 7.5$ nm) and the total porosity (Table I). In the case of the powder W, in which each granule can be considered as one big agglomerate taken from granule G, only 7 vol % of the pores had diameters greater than 7.5 nm, and this is the reason for the absence of a distinct pore population in the pore size distribution curve for sample W, as shown in Fig. 5. The porosity of the agglomerates in G was 40.6 ± 3.7% [16], which

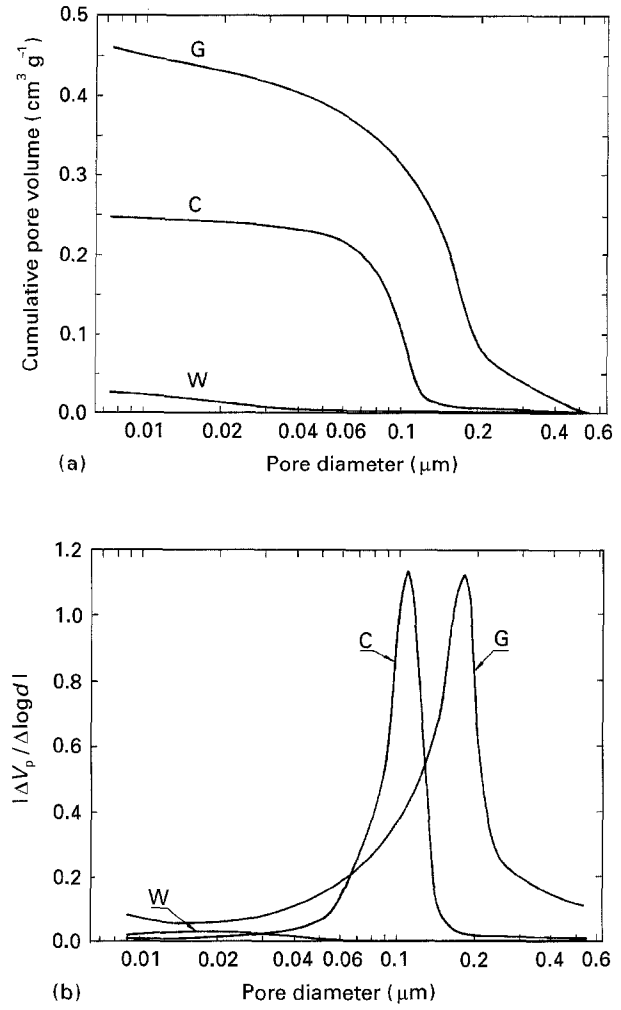

Figure 5 Pore size distribution curves of the "as-spray dried" powders: (a) cumulative curve, (b) derivative plot, $\Delta V_p/\Delta \log d$.

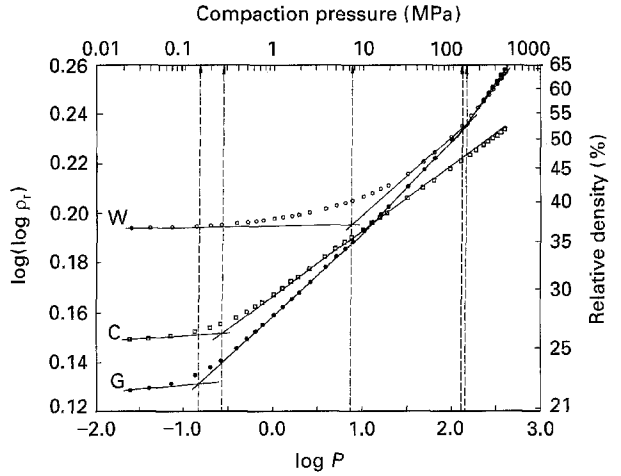

Figure 6 Compaction curves for the "as-spray-dried" powders.

is close to the total porosity of the granules in sample W ($33.0 \pm 0.8\%$). The apparent difference in the cumulative pore volumes measured for samples C and G is due to the system of units used, which could not take into account the difference in real densities of the amorphous gel (3.71 g cm^{-3}) and the crystalline material (6.07 g cm^{-3}). If this is taken into account then sample G is similar to C.

The compaction curves for the powders are shown in Fig. 6, which shows a large difference in strength between the powders. This arises from the large difference in apparent densities of the granules and the size of the particles within the granules (Table I). This difference can be predicted from theory, as shown below.

An early theory for agglomerate strength based on the well known equation for the van der Waals' attractive force, F_{att}, between two spheres of diameter, D, separated by a distance, L, in terms of the Hamaker constant, A (10^{-9} J), was developed by Rumpf [17]. By summing these forces for a particle assembly of volume fraction, ϕ, he obtained the strength, σ, of the agglomerate as

$$\sigma = \frac{1.1\,\phi}{(1-\phi)}\frac{F_{att}}{D^2} = \frac{1.1\,\phi}{(1-\phi)}\frac{A}{24L^2D} \quad (1)$$

Equation 1 shows the important part played by the particle packing; poor packing, which means the larger porosity produces poor agglomerate strength. The importance of very fine particle sizes is anticipated by Equation 1, because of the inverse dependence on particle diameter, D.

A new theory based on fracture mechanics analysis has been proposed by Kendall [18], who derived the following equation for the agglomerate strength, σ^*

$$\sigma^* = 15.6\,\phi^4\Gamma_c^{5/6}\Gamma^{1/6}(Dc)^{-1/2} \quad (2)$$

where σ^* is the bending strength of a beam containing a through edge notch of length c, Γ_c is the fracture energy, Γ is the interfacial energy and D is the diameter of clean, smooth spheres from which the beam is composed. This equation shows the stronger influence of packing fraction, ϕ, the weaker dependence on particle diameter, D, and includes the effect of flaw size, c.

The second break points for samples G and W (Fig. 6) can be attributed to the collapse of the gel agglomerates within the granules, and can be taken as evidence for the existence of agglomerate structure in the granules formed from the wet gel (W). The absence of a second break point in the crystalline material (C) is due to the increased strength of the aggregates.

3.2. Heat treated powders

Analysis of X-ray diffraction patterns obtained from yttria–zirconia gel after heating to 500 °C showed the formation of a zirconia solid solution of cubic symmetry. Differential thermal analysis (DTA) measurements showed an exotherm at 444 °C, which may be associated with the crystallization of gel to form this phase.

Monoclinic zirconia, which was present in C as a result of attrition milling the tetragonal powder, was completely removed by heating the powder to above 800 °C.

Heat treatment resulted in a reduction of granule size (Fig. 7), the largest shrinkage was observed in the granules prepared from the predried attrition milled gel (G), which had also the highest original porosity. The smaller shrinkage observed in the granules prepared from the wet gel (W) can be linked with the

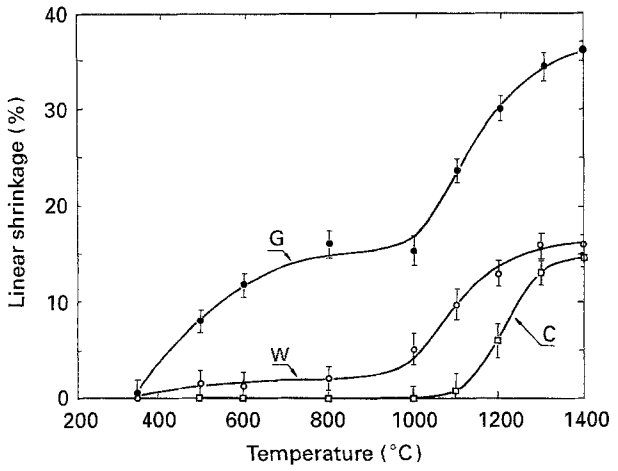

Figure 7 Linear shrinkage of granules versus temperature of heat treatment.

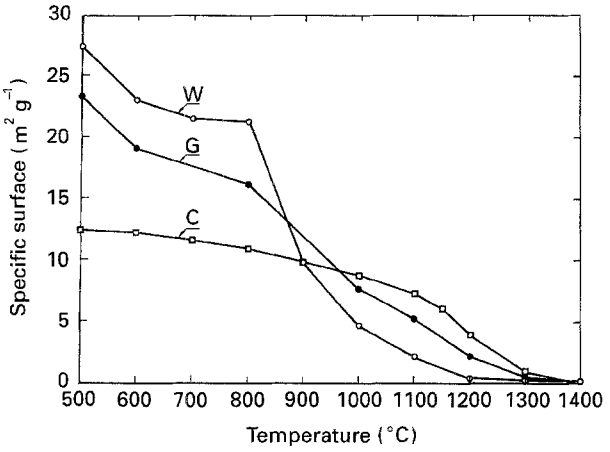

Figure 8 Specific surface area versus temperature of heat treatment.

higher density of the starting granules (67 and 34% for granules W and G, respectively). The granules C, composed of crystalline material, showed even smaller shrinkage, even though the original porosity was high. This was due to the fact that calcination of the powders to 1000 °C prior to milling and spray drying had densified the aggregates, and therefore shrinkage could only commence at temperatures when sintering in between aggregates could occur.

Fig. 8 shows the changes in surface area that accompanied shrinkage. The equivalent particle size, d_{BET} (where BET is Brunauer–Emmett–Teller), together with plots of granule size, crystallite size and agglomerate–aggregate size of the three powders is shown in Fig. 9. In all cases heating to 1400 °C resulted in a reduction in surface area, and a corresponding increase of the equivalent particles size to that approaching the granule size. At temperatures below 800 °C, the coincidence between the equivalent particle size and the crystallite size for G and W indicates that the high specific surface area is controlled by the crystallite size in the agglomerates, whereas in sample C it is the aggregate size which is the controlling factor. The large reduction in surface area exhibited by W indicates that the small crystallites present in originally very dense granules sinter easily, and this

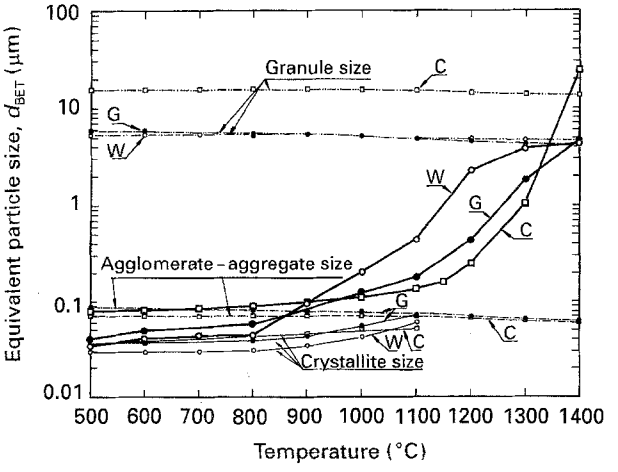

Figure 9 Equivalent particle size, d_{BET}, versus temperature of heat treatment. Changes of the crystallite size, D_{111}, mode of agglomerate–aggregate size, and mode of granule size with temperature are drawn using thinner lines.

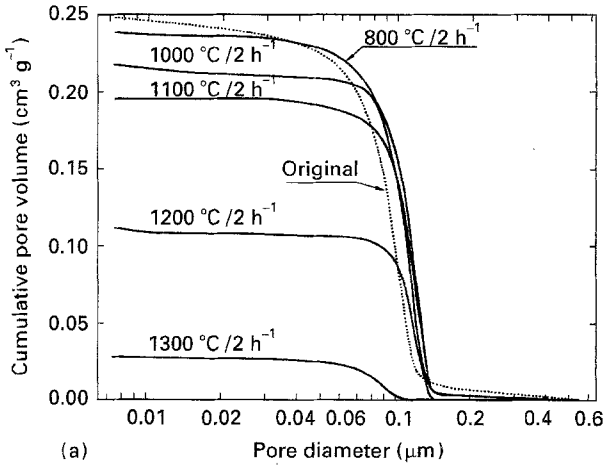

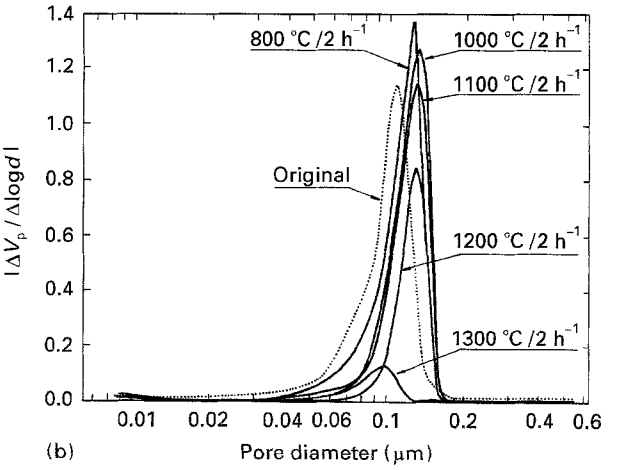

Figure 10 Pore size distribution curves for granules prepared from aggregates of crystalline solid solution (sample C): (a) cumulative curve; (b) derivative plot. Conditions of heat treatment indicated.

results in this sample densifying more rapidly than the other powders.

Details of the sintering behaviour, together with changes in microstructure of these powders during heating can be obtained from analysis of the changes in pore size distributions (Figs 10–12). These show

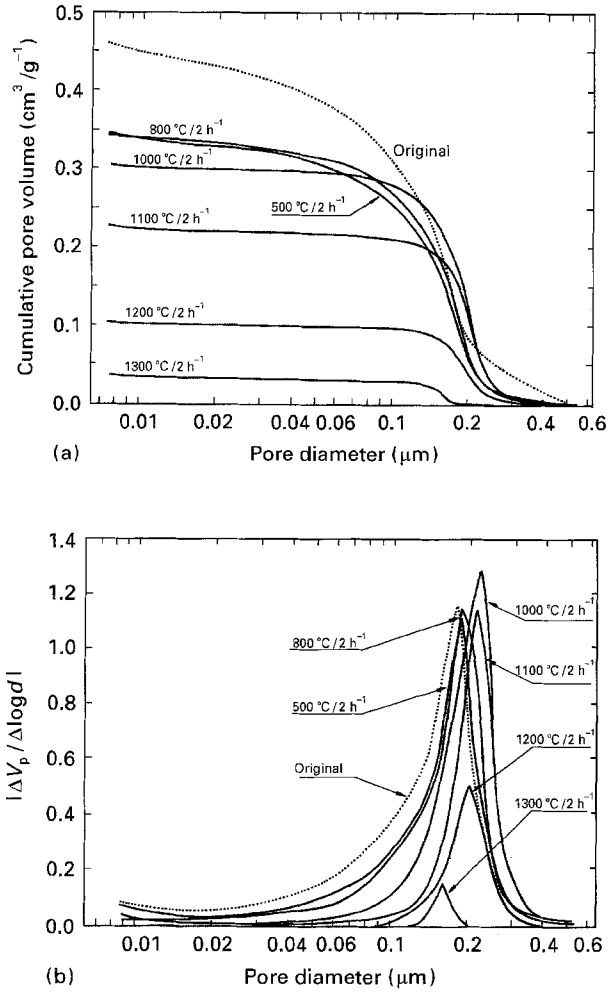

Figure 11 Pore size distribution curves for granules prepared from the water washed, dried and attrition milled gel (sample G): (a) cumulative curve; (b) derivative plot. Conditions of heat treatment indicated.

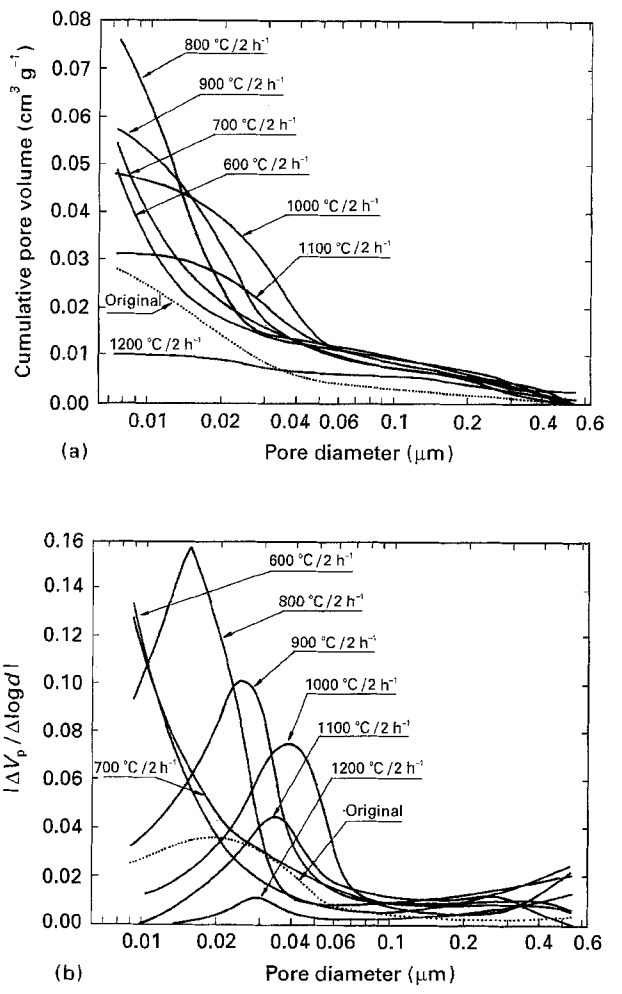

Figure 12 Pore size distribution curves for granules prepared from the wet water washed gel (sample W): (a) cumulative curve; (b) derivative plot. Conditions of heat treatment indicated.

that densification of the granules occurred by the elimination of the smallest pores. At temperatures below those at which rapid shrinkage took place, this was accompanied by an increase in the size of the large pores. Maximum pore growth was observed in the granules prepared from the wet gel (W), as shown in Fig. 12. In all samples this pore growth ceased when rapid shrinkage occurred.

Pore growth during the initial stage of sintering of compacts composed of submicrometre size particles has been reported in a variety of powders [19–21]. The explanation of this phenomenon was given by Lange [22] on the basis of the pore co-ordination number distribution of an agglomerated powder, which defines the particle arrangement within the powder compact. The co-ordination number is the number of touching particles surrounding and defining each pore. The intra-agglomerate pores have a smaller co-ordination number than the interagglomerate pores. According to Lange's concept, during the initial stage of sintering, pores with a co-ordination number, R, smaller than the critical co-ordination number, R_c, can disappear to produce dense regions. As regions densify, some pull away from another, because the local driving force for shrinkage is greater than average. The size of void space between the denser regions and the co-ordination number of these pores increases. If $R > R_c$ the pores cannot shrink without grain growth and/or pore redistribution phenomena that reduce the co-ordination number of pores to values less than R_c.

Pampuch [8] explained the effect of powder packing inhomogenities within the compacts on sintering in the terms of the transient hydrostatic stresses, which arose during sintering, due to the shrinkage rate differential between rapidly shrinking regions (within agglomerates) and slowly shrinking regions (between agglomerates).

Changes of the modal pore size of the granules as a function of temperature are shown in Fig. 13. There is only small pore enlargement within the granules of C. Comparison of the pore size distributions for the granules C with those for the granules G and W indicates that the probable reason for this was the lack of smallest pores in the granules C, due to the calcination process at 1000 °C before attrition milling and spray drying and a very narrow resultant pore size distribution. The presence of a large fraction of pores smaller than 60–80 nm seems to be very important in promotion of growth of the large pores. These pores were formed between single crystallites or between small assemblies of the crystallites. Such domains have

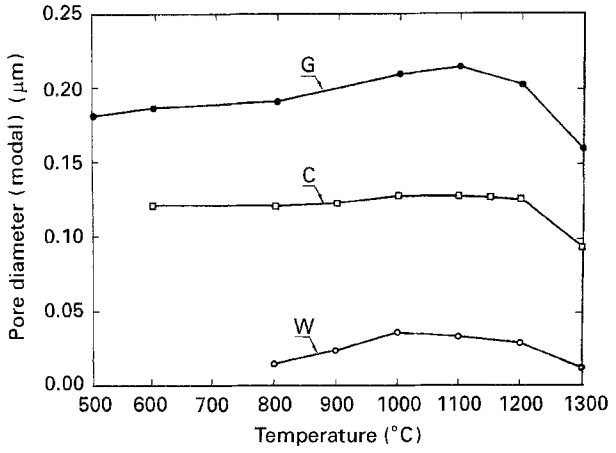

Figure 13 Modal pore diameter versus temperature of heat treatment for samples C, W and G.

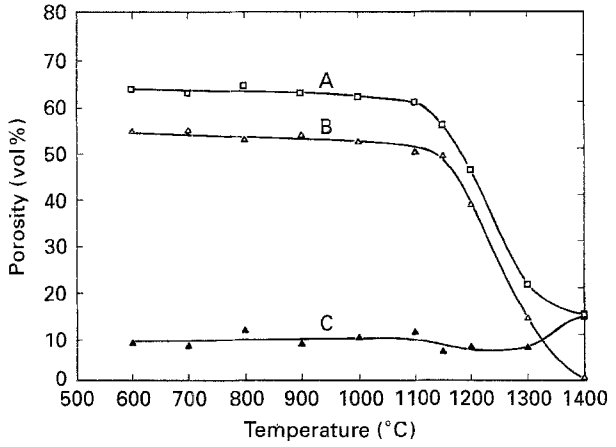

Figure 14 Porosity of the granules prepared from aggregates of crystalline solid solution (sample C) versus temperature of heat treatment: curve A, total porosity; curve B, pores of diameter $\geqslant 7.5$ nm; curve C, curves of diameter < 7.5 nm and/or closed pores.

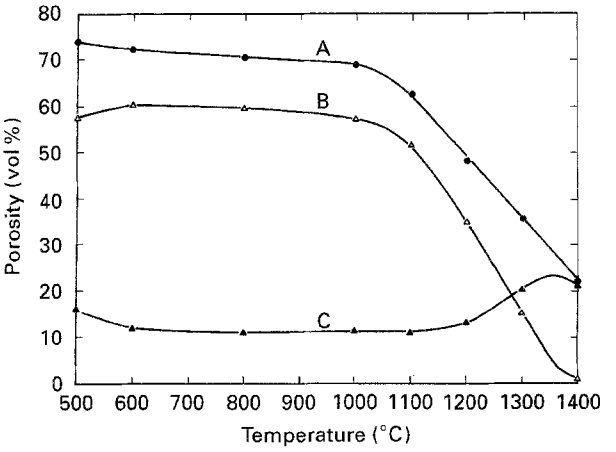

Figure 15 Porosity of the granules prepared from the water washed, dried and attrition milled gel (sample G) versus temperature of heat treatment: curve A, total porosity; curve B, pores of diameter $\geqslant 7.5$ nm; curve C, curves of diameter < 7.5 nm and/or closed pores.

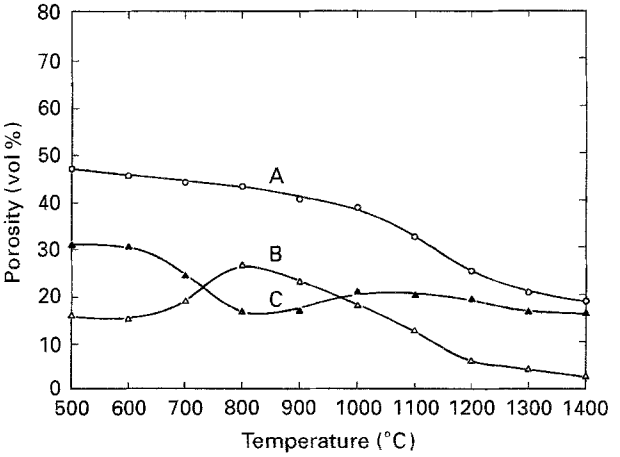

Figure 16 Porosity of the granules prepared from the wet water washed gel (sample W) versus temperature of heat treatment: curve A, total porosity; curve B, pores of diameter $\geqslant 7.5$ nm; curve C, pores of diameter < 7.5 nm and/or closed pores.

a large excess surface energy which is the driving force of sintering, and can densify rapidly at very low temperatures. This is indicated by the volume decrease of the small pores in the pore size distributions shown in Figs 10–12 and the relatively large pore growth within the granules W. The process of pore enlargement ceases at temperatures where the rate of grain growth exceeds the rate of pore growth, i.e. 1000 °C for C and W, and 1100 °C for G.

In Figs 14–16, the vol % of pores of diameter < 7.5 nm, and/or closed pores (curve c), is calculated by subtracting the measured vol % of pores with diameter > 7.5 nm (curve b) from the measured total porosity (curve a). These figures show that there is a very slight decrease in total porosity in the temperature range over which pore enlargement occurred. This indicates that pore enlargement takes place by a redistribution of pores sizes; i.e. elimination of the very fine pores in the agglomerates of samples G and W results in their rapid shrinkage, which, in turn, increases the size of the pores in between the agglomerates. This effect is most apparent in sample W (Fig. 16) at temperatures below 800 °C. The redistribution of pore sizes below 800 °C suggests that the process of surface diffusion and cohesion played a large part in the densification of the regions of the small pore co-ordination number. In all samples, at higher temperatures, there was a decrease in pores of size > 7.5 nm, which was accompanied by a decrease in the total porosity, until at 1400 °C the pores detectable by mercury porosimetry were completely removed and the powders contained only closed pores, or pores < 7.5 nm. The presence of closed porosity in the particles is shown in the scanning electron micrographs (SEM) of the cross-section of the granules in Fig. 17. The large defects in sample W probably originated from inhomogeneous shrinkage which occurred during the spray drying of the wet gel. These defects would also be expected to be responsible for the low compressive strength that was measured in the granules of this powder sintered at 1400 °C (Fig. 18). This is in agreement with Equation 2, which also indicates that the highest values of compressive strength determined for the granules W originated from their highest density over the temperature range up to 1300 °C and from the smallest particles forming

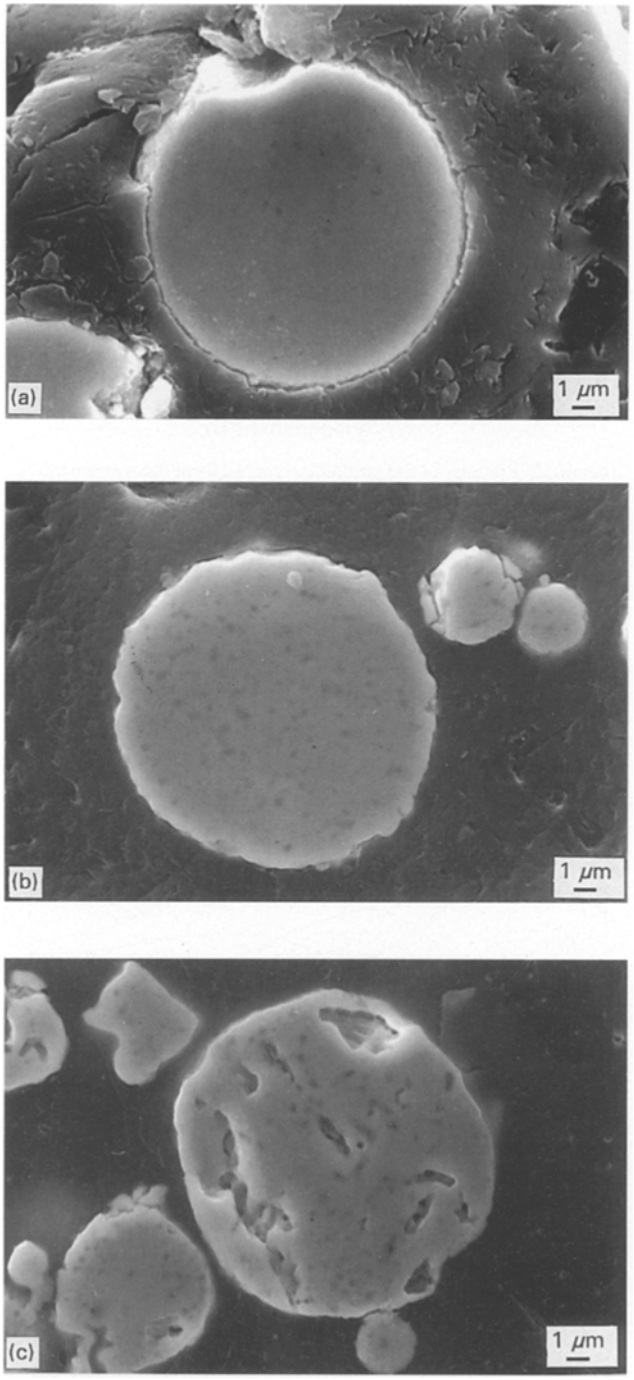

Figure 17 SEM micrographs of the granules sintered at 1400 °C for 2 h: (a) sample C, (b) sample G, and (c) sample W.

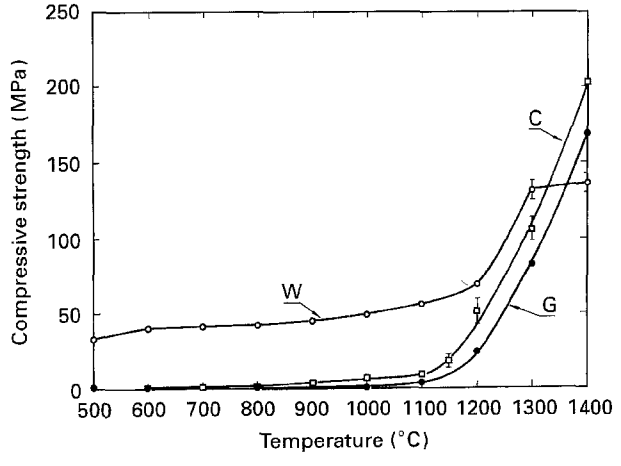

Figure 18 Compressive strength of the granules versus temperature of heat treatment. Samples indicated.

the granules. The flaw size (closed pores) in C is smaller than those in G, and this again is reflected in the higher compressive strength of powder C when compared with G.

4. Conclusions

Three types of yttria–zirconia granules have been characterized (W, G and C). Sample W was composed of granules of dense packed elementary particles of hydrous yttria–zirconia gel, sample G consisted of agglomerates of these elementary gel particles, and C was composed of aggregates of crystalline particles of yttria–zirconia solid solution. The powders were characterized by determining the changes in morphology, specific surface area, pore size distribution, porosity and compressive strength that occurred due to heat treatment.

Prior to heat treatment, the granules of W had the highest density and majority of pores was < 7.5 nm. Both G and C had larger, but comparable, porosities; but the pore size and pore size distributions and surface areas in these two samples differed.

The differences in the original morphologies of the granules affected their behaviour during heat treatment and also their resultant properties. Below 900 °C, the originally amorphous granules of W and G, had higher surface areas than the originally crystalline granules of C, but the latter were more thermally stable, and above 900 °C had the largest surface area.

Local densification by shrinkage of the smallest pores in dense regions of W and G resulted in some pore enlargement during the early stages of sintering, but there was no significant change in the total porosity; thus, the process of pore enlargement was due to a redistribution of pore sizes. The smallest scale of this effect was observed for the granules C, which originally showed a narrow pore size distribution without a significant fraction of pores smaller than 60–80 nm. It was shown that the presence of such pores was responsible for differences in the local densification rate, and promoted pore enlargement in the granules C and W.

The compressive strength of the granules was dependent on the size of the flaws present in the sintered granules. In granules of the powders C and G, this could be related to the size of the closed pores, C having smaller pores and a higher strength. Whereas the low strength of W was attributed to the presence of large flaws which were probably introduced into the granules during the spray drying process of the wet gel.

Acknowledgements

Support was provided under the Generic Technology component of the Industry Research and Development Act 1986. The authors thank L. H. Chen from Centre for Bioprocess Technology, Monash University, for assistance in carrying out measurements.

References

1. W. D. KINGERY, H. K. BOWEN and D. R. UHLMAN, "Introduction to Ceramics", 2nd Edn (Wiley, New York, 1976).

2. M. BERTOLANI, in "Fundamentals of Ceramic Engineering" edited by P. Vincenzini (Elsevier, London, 1991) pp. 27–50.
3. S. NAKA, S. HIRANO, K. KAMIYA, N. YAMAMOTO, S. MATSUZAWA, T. FUJIKAWA and O. KAMIGAITO, in "Fine Ceramics" edited by S. Saito (Ohmsha, Tokyo and Elsevier, New York, 1988) pp. 1–62.
4. A. J. BURGGRAAF and K. KEIZER, in "Inorganic Membranes: Synthesis, Characteristics and Applications", edited by R. Bhave (Van Nostrand Reinhold, New York, 1990) Ch. 2.
5. B. G. LINSEN, (Ed.,) "Physical and Chemical Aspects of Adsorbants and Catalysts" (Academic Press, London, 1970) pp. 1–59, 171–212, 213–264, 265–283, 316–628.
6. J. D. F. RAMSAY, in "Chromatography of Synthetic and Biological Polymers", edited by R. Epton (Ellis Horwood, Chichester, 1977) p. 339.
7. K. HABERKO, *Ceram. Int.* **5** (1979) 148.
8. R. PAMPUCH, in "Advances in Ceramics, Vol. 12, Science and Technology of Zirconia II", edited by N. Claussen, M. Rühle and A. H. Heuer (American Ceramic Society, Columbus, OH, 1984) pp. 733–743.
9. F. F. LANGE, *J. Amer. Ceram. Soc.* **72** (1989) 3.
10. M. T. W. HEARN, M. AQUILAR, Q.-M. MAO and D. VANSELOW, *Aust. Biotech.* **3** (1993) 148.
11. H. P. KLUG and L. E. ALEXANDER, "X-ray Diffraction Procedures" (Wiley, New York, 1954) Ch. 9.
12. S. GASIOREK, in "Science of Ceramics", Vol. 10, edited by H. Hausner (Deutsche Keramische Geselschaft, Berlin, 1980) pp. 311–319.
13. G. L. MESSING, C. J. MARKHOFF and L. G. McCOY, *Amer. Ceram. Bull.* **61** (1982) 857.
14. H. G. SCOTT, *J. Mater. Sci.* **10** (1975) 1527.
15. W. PYDA, M. S. J. GANI and L. H. CHEN, in "Science and Technology of Zirconia V", edited by S. P. S. Badwal, M. J. Bannister and R. H. J. Hannink (Technonic Publ. (O. Lancaster, PA, 1993) pp. 223–229.
16. W. PYDA and M. S. J. GANI, *J. Amer. Ceram. Soc.* submitted.
17. H. RUMPF, *Chem. Ing. Technol.* **30** (1958) 144.
18. K. KENDALL, *Powder Metall.* **31** (1988) 28.
19. O. J. WHITTEMORE, Jr and J. J. SIPE, *Powder Technol.* **9** (1974) 159.
20. J. LIS and R. PAMPUCH, in "Proceedings of the Ceramic Committee of Polish Academy of Science", **36** (Polish Academy of Science, Cracow 1988) p. 7.
21. F. F. LANGE and B. I. DAVIES, in "Advances in Ceramics, Vol. 12, Science and Technology of Zirconia II", edited by N. Claussen, M. Rühle and A. H. Heuer (The American Ceramic Society, Columbus, OH, 1984) pp. 699–713.
22. F. F. LANGE, *J. Amer. Ceram. Soc.* **67** (1984) 83.

Received 5 August 1993
and accepted 8 September 1994